Strongly Magnetized Antihydrogen and Its Field Ionization

D. Vrinceanu,[1] B. E. Granger,[1] R. Parrott,[2] H. R. Sadeghpour,[1] L. Cederbaum,[1,3] A. Mody,[2] J. Tan,[2] and G. Gabrielse[2]
[1]*ITAMP, Harvard-Smithsonian Center for Astrophysics, Cambridge, Massachusetts 02138, USA*
[2]*Department of Physics, Harvard University, Cambridge, Massachusetts 02138, USA*
[3]*Theoretische Chemie Physikalisch-Chemisches Institut, Heidelberg, Germany*
(Received 30 September 2003; published 31 March 2004)

Internal orbits of experimentally analyzed antihydrogen ($\overline{\mathrm{H}}$) atoms depend as much on an external magnetic field as on the Coulomb force. A circular "guiding center atom" model is used to understand their field ionization. This useful model, assumed in the theory of three-body $\overline{\mathrm{H}}$ recombination so far, ignores the important coupling between internal and center-of-mass motion. A conserved pseudomomentum, effective potential, saddle point analysis, and numerical simulation show where the simple model is valid and classify the features of the general case, including "giant dipole states."

DOI: 10.1103/PhysRevLett.92.133402 PACS numbers: 36.10.–k

Observations of slow $\overline{\mathrm{H}}$ atoms [1–3] bring closer the exciting prospect of $\overline{\mathrm{H}}$ cold enough to be trapped and precisely compared to H [4], building upon the laser spectroscopy of H [5]. Slow $\overline{\mathrm{H}}$ production takes place during the positron (e^+) cooling of antiprotons ($\overline{p}$) in a nested Penning trap [6], which intrinsically includes a strong magnetic field. To demonstrate that $\overline{\mathrm{H}}$ was produced, ATHENA counted e^+ and $\overline{p}$ annihilations taking place within ± 8 mm and 5 μs [1]. ATRAP field ionized the $\overline{\mathrm{H}}$ and counted the $\overline{p}$ that were liberated by ionization and then trapped [2,3]. This method also probes the internal $\overline{\mathrm{H}}$ orbits, knowledge of which is required to devise ways to deexcite $\overline{\mathrm{H}}$ for trapping and spectroscopy.

Of interest here are the general theoretical questions raised by field ionization of $\overline{\mathrm{H}}$ in a strong magnetic field. For electric and magnetic fields $F\mathbf{z}$ and $B\mathbf{z}$ in direction $\mathbf{z}$, what does field ionization reveal about the $\overline{\mathrm{H}}$ binding energy and size? How does the coupling between center-of-mass (c.m.) and internal motion affect field ionization? This Letter first explores $\overline{\mathrm{H}}$ field ionization using a simple, useful model, then provides a more general framework applicable to classical (and quantum) calculations of excited $\overline{\mathrm{H}}$ states in a strong $\mathbf{B}$ field. A conserved pseudomomentum [7–10] leads to an equation of motion for the internal $\overline{\mathrm{H}}$ motion in which the important coupling of the internal and c.m. motion is contained in an offset harmonic potential. Saddle point analysis and numerical simulation reveal general features of the ionization.

The nonintegrable internal motion of a Rydberg atom in a strong $\mathbf{B}$, following one and two photon excitations from the ground state [11,12], was successfully analyzed with semiclassical methods [13], large scale quantum calculations [14], and random matrix theory [15]. However, three-body $\overline{\mathrm{H}}$ formation [16–18] produces a greater variety of states, higher angular momenta, and significant motion perpendicular to the magnetic field.

A $\overline{p}$ within an e^+ plasma at a low temperature T will most readily form $\overline{\mathrm{H}}$ via the three-body process $\overline{p} + e^+ + e^+ \rightarrow \overline{\mathrm{H}} + e^+$ [16]. A e^+ (mass $m = m_+$ and charge e) is initially captured into a large orbit about the $\overline{p}$ (mass m_- and charge $-e$) with a size of order of $b = r_e mc^2/(kT)$, the separation at which the thermal and Coulomb energies are equal for two elementary charges; r_e is the classical electron radius. $\overline{\mathrm{H}}$ atoms then deexcite towards the desired ground atomic state via replacement [17] and diffusion collisions [18] until leaving the e^+ plasma. An electric field $F\mathbf{z}$ that turns on adiabatically is intended to ionize and analyze the size and energy of the $\overline{\mathrm{H}}$ atoms.

One limit for the $\overline{\mathrm{H}}$ formed is obtained in the guiding center approximation (GCA) [19] in which the e^+ makes cyclotron, axial, and magnetron motions much like a particle in a Penning trap [20]. Rapid e^+ cyclotron motion at angular frequency $\omega_c = eB/m$ is treated as a negligibly small magnetic moment at its "guiding center" [19], and the cyclotron kinetic energy E_c is essentially conserved. The center oscillates axially along $\mathbf{z}$ at angular frequency ω_z; the ratio of the axial energy and ω_z is an adiabatic invariant. The drift or magnetron motion, at angular frequency ω_m, has a transverse velocity, $\dot{\boldsymbol{\rho}} = -\nabla V \times \mathbf{z}/B$, dependent only on the electric and magnetic fields, to both of which it is perpendicular. The drift kinetic energy is negligibly small. Drift orbit size, rather than energy, best characterizes GCA atoms since a large energy can be stored in tiny cyclotron orbits with little consequence.

The first of two GCA conditions is a $\rho = |\boldsymbol{\rho}|$ (e.g., Fig. 1) much larger than the cyclotron radius, where $\mathbf{r} = x\mathbf{x} + y\mathbf{y} + z\mathbf{z} = \boldsymbol{\rho} + z\mathbf{z}$ is the position of the e^+ relative to the $\overline{p}$. For a thermal e^+ velocity $v_e = \sqrt{2kT/m}$, this requires $\rho \gg v_e/\omega_c = 0.01$ μm for 4.2 K. Second, the internal oscillations must differ in time scale so that $\omega_c \gg \omega_z \gg \omega_m$, as is familiar for a particle in a Penning trap [20]. This corresponds to $\rho \gg (r_e c^2/\omega_c^2)^{1/3} = 0.04$ μm for ATRAP's $B = 5.3$ T for the frequencies of the special case discussed next. When these conditions are not met, the nonintegrable motion

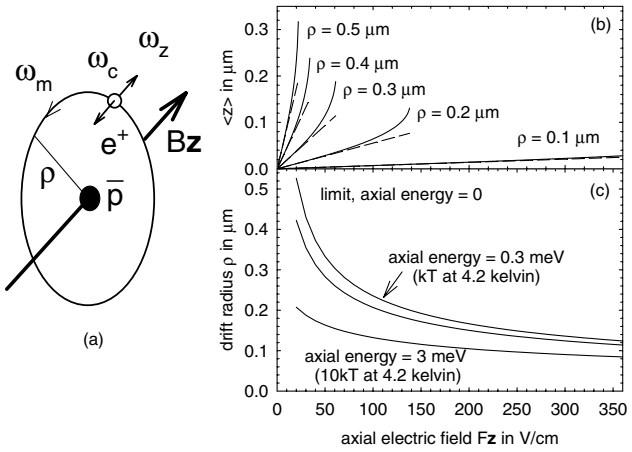

FIG. 1. A circular guiding center $\overline{\mathrm{H}}$ atom (a) is polarized (b) and ionized (c) by an electric field **F** is applied along **B**.

in similar strength magnetic and Coulomb fields allows for chaotic orbits [15].

The important special case is the circular GCA atom [Fig. 1(a)] used to calculate rates for three-body formation of magnetized $\overline{\mathrm{H}}$ [17,18] and for radiation from circular Rydberg states [21], for an axially symmetric $V \sim 1/r$ with no $\overline{\mathrm{H}}$ c.m. motion transverse to **B**. The angular frequency for small axial oscillations ($z \ll \rho$) is $\omega_z = \sqrt{r_e c^2/\rho^3}$, and the angular drift frequency is $\omega_m = r_e c^2/(\omega_c \rho^3)$. The axial adiabatic invariant means that the axial energy $E_z \sim \omega_z \sim \rho^{-3/2}$ for small z. The guiding center of an $\overline{\mathrm{H}}$ formed with axial energy E_{z0} at $\rho = \rho_0$ then follows an orbit given by $E_{z0}(\rho_0/\rho)^{3/2} + V(z = 0) = \text{const}$ in this limit.

Circular GCA atoms are polarized or ionized by $F\mathbf{z}$ in a way that depends upon their radial size ρ, but without changing ρ. As $F\mathbf{z}$ is adiabatically added to the Coulomb potential, the calculated center of the axial oscillation of the e^+ moves to stay centered in the resultant axial potential well [the solid curves in Fig. 1(b)]. (For ATRAP F changes adiabatically insofar as $\overline{\mathrm{H}}$ move slowly into the ionization field.) This $\overline{\mathrm{H}}$ polarizability can be calculated analytically for F small enough that the average $\bar{z} \ll \rho$. The average induced dipole is then $e\bar{z} = \alpha F$, with a polarizability $\alpha \approx e^2\rho^3/(r_e mc^2)$ [dashes in Fig. 1(b)].

If we relaxed our assumption that **F** is spatially uniform, the force on the induced dipole, $(\alpha/2)(\partial/\partial z)F^2$ in the linearized case, would provide a 1D restoring force on the $\overline{\mathrm{H}}$ to any point for which F^2 is maximum along **z**. At the origin, a field $F \sim \cos az$ will provide such confinement whereas a harmonic $F \sim z$ will not.

A polarized $\overline{\mathrm{H}}$ ionizes when its e^+ is able to escape the axial well, which eventually vanishes as F increases. An $\overline{\mathrm{H}}$ that survives F thus has ρ smaller than

$$\rho = \frac{a}{\sqrt{F}}\sqrt{\frac{e}{4\pi\epsilon_o}}, \tag{1}$$

with $a = (4/27)^{1/4} \approx 0.62$ [Fig. 1(c)] and Coulomb constant $4\pi\epsilon_0$. The square root constant is 1 a.u. and 3.795 $\mu\mathrm{m}\sqrt{\mathrm{V/cm}}$. An e^+ with axial energy is ionized by a smaller F [e.g., Fig. 1(c) for axial energies of kT and $10kT$ for $T = 4.2$ K]. A thermal distribution of e^+ axial energies is predicted due to collisions with other e^+ [17]; for axial energy much less than the radial binding energy, $|E_b| \sim 1/\rho$, the limit Eq. (1) is $|E_b| = \sqrt{F}/a\sqrt{e^3/(4\pi\epsilon_o)}$, where this square root constant is 1 a.u. and 0.3795 $\mathrm{meV}\sqrt{\mathrm{cm/V}}$. Quantum tunneling from the axial well in the 100 μs or less that $\overline{\mathrm{H}}$ travel from production to detection only slightly lowers the curves of Fig. 1(c).

Determining where the simple circular model is valid, and improving upon it, requires an analysis that includes the motion of the $\overline{\mathrm{H}}$ c.m., with mass M at position **R**, neglected so far. The key is a pseudomomentum [7,8]

$$\mathbf{K} \equiv M\dot{\mathbf{R}} - e\mathbf{r} \times \mathbf{B}, \tag{2}$$

which is conserved along with the total energy, which now is the sum of the energy in the relative and c.m. motions. K_z is the c.m. momentum parallel to **B**. Without loss of generality we choose **y** so that $\mathbf{K}_\perp = K_\perp \mathbf{y}$. For us, $K_\perp$ distinguishes different types of $\overline{\mathrm{H}}$ states; earlier it was useful in characterizing how c.m. motion was affected as internal atomic motion became chaotic [9,10].

A simple model estimates the $K_\perp$ distributions that might be expected for formation and deexcitation of $\overline{\mathrm{H}}$ (Fig. 2), consistent with a recent simulation [22]. We associate a binding energy βkT with a radius $r = b/\beta$ as would pertain for circular atoms. For three-body formation of $\overline{\mathrm{H}}$, a capture and deexcitation through a "bottleneck" at $\beta \approx 4$ is predicted [17]. The $K_\perp$ distribution arises from a thermal distribution of c.m. velocities and a random distribution of $\boldsymbol{\rho}$; the basic features do not change if we populate an area of radius b/β transverse to **B**, a shell of this radius (in Fig. 2), or the interior of this shell, so that $K_\perp < 1$ a.u. is expected.

The conservation of **K** is established directly by the first of two equations of motion for $\overline{\mathrm{H}}$ in uniform magnetic and electric fields, **B** and **F**,

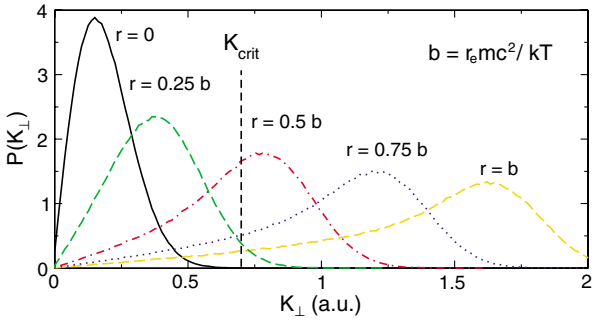

FIG. 2 (color). Estimated pseudomomentum $K_\perp$ distributions for $\overline{\mathrm{H}}$ production within a 4.2 K e^+ plasma. For $K_\perp > K_{\mathrm{crit}}$ giant dipole states can exist as we discuss.

$$0 = \frac{d}{dt}[M\dot{\mathbf{R}} - e\mathbf{r} \times \mathbf{B}] \equiv \frac{d\mathbf{K}}{dt}, \tag{3}$$

$$\mu\ddot{\mathbf{r}} = e\dot{\mathbf{R}} \times \mathbf{B} + e\dot{\mathbf{r}} \times \lambda\mathbf{B} - \frac{e^2}{4\pi\epsilon_o}\frac{\mathbf{r}}{r^3} - e\mathbf{F}. \tag{4}$$

Here μ is the familiar reduced mass, and $\lambda = (m_- - m_+)/M$ would vanish for $m_- = m_+$ (e.g., positronium).

Using the conserved $\mathbf{K}$ to eliminate explicit references to the c.m. motion [9] from Eq. (4) yields an equation involving only the relative coordinates,

$$\mu\ddot{\mathbf{r}} = -\nabla V(\mathbf{r}) + e\dot{\mathbf{r}} \times \lambda\mathbf{B}, \tag{5}$$

for a charge e and mass μ in an effective magnetic field $\lambda\mathbf{B} \approx \mathbf{B}$ and an effective potential

$$V(\mathbf{r}) = \frac{1}{2}M\Omega_c^2(\boldsymbol{\rho} - \mathbf{x_o})^2 - \frac{1}{4\pi\epsilon_0}\frac{e^2}{r} - e\mathbf{F} \cdot \mathbf{r}. \tag{6}$$

Coupling to the c.m. motion is completely described by the harmonic term with an offset $\mathbf{x}_0 \equiv K_\perp\hat{\mathbf{x}}/(eB)$ and a strength given by $\Omega_c = eB/M$—nearly the $\overline{p}$ cyclotron frequency. Figure 3 shows equipotentials and projections of $V(\mathbf{r})$ for $K_\perp = 1$ a.u. As $K_\perp$ increases above $K_{\rm crit} = 3e[MB/(16\pi\epsilon_0)]^{1/3}$, a giant dipole well emerges as a consequence of the coupling to the c.m. motion [10].

The relative equation of motion corresponds to a conserved Hamiltonian, $H = \frac{1}{2}\mu\dot{\mathbf{r}}^2 + V(\mathbf{r})$ [10], where $\mu\dot{\mathbf{r}} = \mathbf{p} - e\mathbf{A}(\mathbf{r})$ is related to the canonical momentum $\mathbf{p}$ and the vector potential $\mathbf{A}$ in the usual way. The internal $\overline{H}$ energy is $E_{\rm rel} = \frac{1}{2}\mu\dot{\mathbf{r}}^2 - e^2/(4\pi\epsilon_0 r)$. The alternate form, $H = \frac{1}{2}M\dot{\mathbf{R}}_\perp^2 + E_{\rm rel}$, emphasizes that total energy is conserved while $E_{\rm rel}$ is not.

Figure 4 illustrates different types of regular drift orbits. The GCA is valid over the area shown, except very close to the Coulomb center (+), where $\rho < 0.25$ μm as we shall see. First, just outside this radius but still within the Coulomb well, the GCA orbits are nearly circular, becoming more elliptical with increasing size. Second, an unusual class of nearly circular GCA states with large electric dipole moments oriented perpendicular to $\mathbf{B}$ form in the very shallow giant dipole well. These states are ionized before leaving the nested Penning trap within which they form, by electric fields that exceed 2 V/cm. Third, noncircular guiding center orbits nearly follow equipotentials that encircle both the Coulomb well and the displaced giant dipole well, but these too have weak axial binding energies and are easily ionized. Fourth, but not shown, are orbits that can be chaotic as they closely approach the Coulomb center.

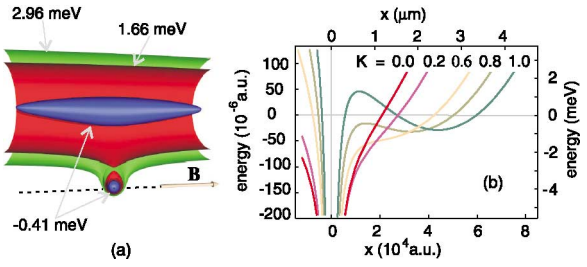

FIG. 3 (color). (a) Three equipotential surfaces of $V(\mathbf{r})$ for $B = 5.4$ T, $K_\perp = 1$ a.u., and $F = 0$. (b) Effective potential $V(x, y = 0, z = 0)$ along the x axis for various values of $K_\perp$.

A saddle point analysis seems appropriate for these smaller orbits. The first manifestations of the onset of chaos are close collisions which transfer energy between cyclotron, axial, and drift motions, making rather sudden changes in the e^+ orbit. These motions become completely entangled for smaller ρ, the chaotic orbits eventually filling the energetically allowed phase space. The atom size is then the radius of the xy region bounded by the equipotential going through the saddle point for V [dashes in Fig. 5(g)] and approaching Eq. (1) with $a = 1/2$ with increasing F. In the limit of smaller atom sizes and larger ionization fields, unlike the GCA for larger atoms and smaller ionization fields, conservation of total energy gives a limit to the size of the atom that increases with increasing energy.

Numerical simulations confirm the general features that have been described. For various adiabatically applied electric fields, trajectories started from the initial x and y values in Figs. 5(a)–5(f) with $\dot{x} = \dot{y} = 0$ are not field ionized for more than 10^3 cyclotron periods (7 ns). The effective radii of these stable regions are represented by the points in Fig. 5(g). More familiar ionization for $B = 0$ [23] is recovered in Figs. 5(a) and 5(g) for which $K_\perp = 0$.

These different approaches give much the same result for the smaller radii and larger ionization fields for which c.m. motion and $K_\perp$ become increasingly less relevant. The encouraging conclusion is that field ionization and Fig. 5(g) should give a reliable indication of $\overline{\rm H}$ size for electric fields that can be readily applied in the laboratory, even for smaller sized atoms which have chaotic orbits.

For c.m. motion, the conservation of $\mathbf{K}$ suggests that c.m.trajectories are ballistic on average for thermal $\overline{\rm H}$

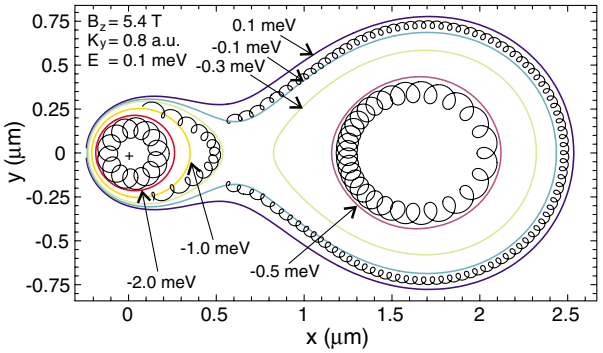

FIG. 4 (color). Radial orbit examples superimposed on radial equipotentials of $V(\mathbf{r})$ for $K_\perp = 1$ a.u. Cyclotron radii have been increased and the cyclotron frequency decreased to make them visible.

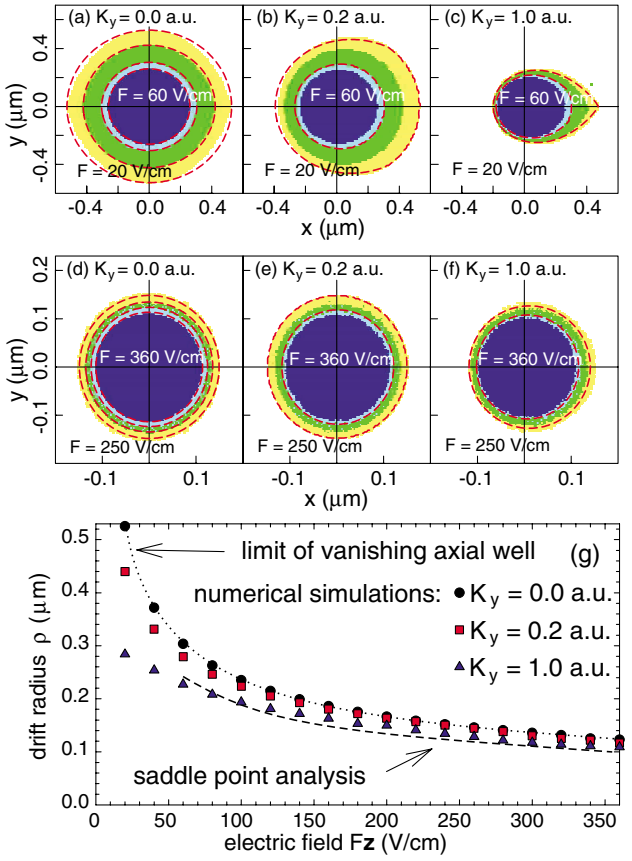

FIG. 5 (color). Numerical simulations for $z = 0$ identify $\overline{\mathrm{H}}$ orbits that are stable against ionization by $F\mathbf{z}$ applied adiabatically for various values of $K_\perp = k_y$ and F in (a)–(f). $\overline{\mathrm{H}}$ surviving a field F must have radii lower than that shown in (g).

velocities and reasonably small $K_\perp$ despite the coupling to relative motion, as confirmed by simulations [22]. Both $\mathbf{r} \times \mathbf{B}$ and $\dot{\mathbf{R}}$ in Eq. (2) oscillate at relative oscillation frequencies to keep $\mathbf{K}$ independent of time. Since the corresponding periods are short compared to the transit time of an $\overline{\mathrm{H}}$ through the apparatus, the effect of these oscillations on the c.m. motion averages away.

Spatial gradients in $\mathbf{F}$ (e.g., due to the relatively weak fields of the nested Penning trap) have not been included in our analysis. Doing so adds $e\mathbf{r} \cdot \nabla' \mathbf{F}(\mathbf{r}')|_{\mathbf{r}'=\mathbf{R}}$ to the right of Eq. (3), and the sum of this term and $e\mathbf{F}(\mathbf{R})$ replace $e\mathbf{F}$ in Eq. (5). $\mathbf{K}_\perp$ is not conserved and coupled equations for the c.m. and relative motion must be solved. Fields from harmonic potentials are simple in that the gradient terms are independent of $\mathbf{R}$, but $\mathbf{K}_\perp$ is still not conserved and $\mathbf{F}(\mathbf{R})$ still couples the relative and c.m. equations. For the special case $F(z)\mathbf{z}$ (e.g., for ATRAP $\overline{\mathrm{H}}$ traveling into the prestripping field), $\mathbf{K}_\perp$ is conserved and Eq. (5) is unchanged. The coupled c.m. and relative axial equations describe the polarization of the $\overline{\mathrm{H}}$ and the force on this induced moment; for ATRAP this slightly speeds the $\overline{\mathrm{H}}$ motion to the detection well.

In conclusion, a conserved pseudomomentum allows the analysis of coupled internal and c.m. motions for magnetized $\overline{\mathrm{H}}$ atoms and provides a general framework for improved classical and quantum calculations of the formation of such atoms. A classical analysis shows that $\overline{\mathrm{H}}$ c.m. motion in a strong $\mathbf{B}$ produces unusual internal $\overline{\mathrm{H}}$ orbits, some with large electric dipoles. This general approach shows that a simple circular atom model, combined with a saddle point analysis and numerical simulations, gives a consistent picture of the relationship between the size of an $\overline{\mathrm{H}}$ and the field that ionizes it, thus supporting the usefulness of the ATRAP field ionization method. The analysis shows that orbits with large electric dipoles ionize so easily that they have not yet been observed experimentally, and that the coupling between $\overline{\mathrm{H}}$ center-of-mass and internal motion is less of a complication for $\overline{\mathrm{H}}$ moving along the magnetic field direction, the configuration used by ATRAP.

This work was supported by NSF, AFOSR, and ONR.

[1] M. Amoretti *et al.*, Nature (London) **419**, 456 (2002).
[2] G. Gabrielse *et al.*, Phys. Rev. Lett. **89**, 213401 (2002).
[3] G. Gabrielse *et al.*, Phys. Rev. Lett. **89**, 233401 (2002).
[4] G. Gabrielse, in *Fundamental Symmetries*, edited by P. Bloch, P. Paulopoulos, and R. Klapisch (Plenum, New York, 1987), p. 59.
[5] C. Zimmerman and T.W. Hänsch, Hyperfine Interact. **76**, 47 (1993).
[6] G. Gabrielse *et al.*, Phys. Lett. B **507**, 1 (2001).
[7] B. P. Carter, J. Math. Phys. (N.Y.) **10**, 788 (1969).
[8] J. E. Avron, I.W. Herbst, and B. Simon, Ann. Phys. (N.Y.) **114**, 431 (1978).
[9] P. Schmelcher and L. S. Cederbaum, Comments Mod. Phys. D **2**, 123 (2000).
[10] O. Dippel, P. Schmelcher, and L. S. Cederbaum, Phys. Rev. A **49**, 4415 (1994).
[11] G. Littman, M. M. Kash, and D. Kleppner, Phys. Rev. Lett. **41**, 103 (1978).
[12] J. Main, G. Wiebusch, A. Holle, and K. H. Welge, Phys. Rev. Lett. **57**, 2789 (1986).
[13] M. L. Du and J. B. Delos, Phys. Rev. A **38**, 1896 (1988).
[14] C.W. Clark and K. T. Taylor, J. Phys. B **13**, L737 (1980).
[15] D. Delande and J. C. Gay, Phys. Rev. Lett. **57**, 2006 (1986).
[16] G. Gabrielse, S. L. Rolston, L. Haarsma, and W. Kells, Phys. Lett. A **129**, 38 (1988).
[17] M. Glinsky and T. O'Neil, Phys. Fluids B **3**, 1279 (1991).
[18] P. O. Fedichev, Phys. Lett. A **226**, 289 (1997).
[19] B. Lehnert, *Dynamics of Charged Particles* (Wiley, New York, 1964).
[20] L. S. Brown and G. Gabrielse, Rev. Mod. Phys. **58**, 233 (1986).
[21] J. R. Guest, J.-H. Choi, and G. Raithel, Phys. Rev. A **68**, 022509 (2003).
[22] F. Robicheaux (private communication).
[23] T. F. Gallagher, *Rydberg Atoms* (Cambridge University Press, New York, 1994).